Unraveling the Electric Field-Induced Second Harmonic Generation Responses of Stilbazolium Ion Pairs Complexes in Solution Using a Multiscale Simulation Method

Ramos, Tárcius N.; Champagne, Benoît; Canuto, Sylvio

Published in:
Journal of chemical information and modeling

DOI:
10.1021/acs.jcim.9b01161

Publication date:
2020

Document Version
Publisher's PDF, also known as Version of record

JCIM JOURNAL OF CHEMICAL INFORMATION AND MODELING

pubs.acs.org/jcim Article

Unraveling the Electric Field-Induced Second Harmonic Generation Responses of Stilbazolium Ion Pairs Complexes in Solution Using a Multiscale Simulation Method

Tárcius N. Ramos, Sylvio Canuto, and Benoît Champagne*

Cite This: J. Chem. Inf. Model. 2020, 60, 4817−4826 Read Online

ACCESS | Metrics & More | Article Recommendations | Supporting Information

ABSTRACT: The electric field-induced second harmonic generation (EFISHG) response has been largely used to describe the first β and the second γ hyperpolarizabilities in solution. Although the EFISHG technique cannot be applied to charged compounds (due to the external static electric field), it can be used to describe ion pairs as neutral complexes. A multiscale computational approach is required to generate representative geometrical configurations of such kinds of complexes (using classical force fields), to compute the electronic structure of each configuration (using quantum mechanics methods), and to perform statistical analyses describing the behavior of the nonlinear optical properties. In this work, we target solvated neutral ion pairs complexes, of which the cation is an organic chromophore, and we estimate their EFISHG and hyper-Rayleigh scattering responses. It is shown that the anion−cation relative spatial distribution determines the permanent dipole moment of the complexes, and therefore the relative distance controls the EFISHG response. On the other hand, the β tensor is independent of the dipole moment and it shows a weak linear correlation with the π-electron conjugation length of the cations. The γ contributions in the global EFISHG response range from 5% to 15%, which is mostly due to the variations of amplitude of the $\mu\beta_{\parallel}$ contribution, which results from differences in the μ and β vectors' orientations. The applied multiscale approach provides reasonable results compared with experimental ones, although additional efforts are still required to improve such comparison mainly to consider the possible dissociation effects.

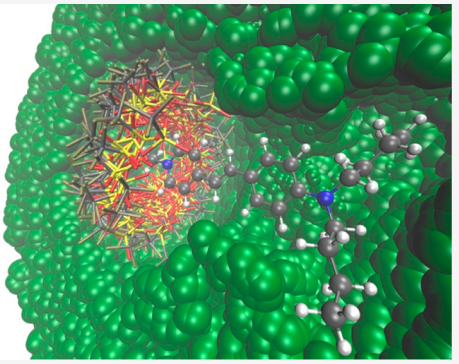

1. INTRODUCTION

Nonlinear optics deals with those phenomena where matter modifies the properties of light and *vice versa*.[1] Among these phenomena, the second harmonic generation (SHG) response has been used to tune the frequency of laser light, to perform bioimaging,[2] and to design molecular-scale logic devices.[3] Other phenomena encompass an intensity-dependent refractive index, employed in self-focusing applications, and two-photon absorption (TPA), used in optical power limiting,[4] bioimaging,[5] and microfabrication.[6] An important and often preliminary aspect for better understanding the light-matter interactions is, therefore, the characterization of the global nonlinear optical (NLO) responses of matter as well as their tensor components.

The electric field-induced second harmonic generation (EFISHG) technique is a well-known technique to determine the first β and the second γ hyperpolarizabilities of compounds in solutions. To perform such measurements, an external electrostatic field is applied to the sample in order to break the isotropicity and therefore to create preferential molecular orientations. Consequently, EFISHG probes the vector component of β along the molecular dipole moment, while it cannot be employed to investigate charged compounds.[7] However, besides many applications to neutral molecules, the EFISHG technique has recently been used for determining the NLO responses of neutral complexes composed by anion−cation pairs. Still, to investigate these neutral complexes in solution, the use of low dielectric constant solvents, such as $CHCl_3$, is required to favor ion pairing and avoiding the undesired dissociation. This was first demonstrated in 2000 for amphiphilic polyenic push−pull chromophores[8] and recently applied to pH-triggered NLO switches.[9] Though EFISHG measurements have already been reported for ion pairs, few theoretical modeling studies have been done to describe the EFISHG responses of such kinds of complexes in solution.[10] Subsequently, little is known about the effect of the nature of the charged species (both the chromophore and its counterion) on the EFISHG response. Indeed, accounting for thermal and surrounding effects on the NLO responses of these complexes remains challenging.

Received: December 15, 2019
Published: April 13, 2020

https://dx.doi.org/10.1021/acs.jcim.9b01161
J. Chem. Inf. Model. 2020, 60, 4817−4826

In this work, following the experimental investigation of Tessore et al.,[11] the relationship between the geometrical structures and the EFISHG responses are evaluated for complexes composed by stilbazolium cations and small- to medium-sized anions (from the inorganic iodide to the organic *p*-toluenesulfonate). The stilbazolium cations present large second-order NLO responses due to their push−pull π-conjugated character. The chemical structures of the complexes are presented in Figure 1. Contrary to the

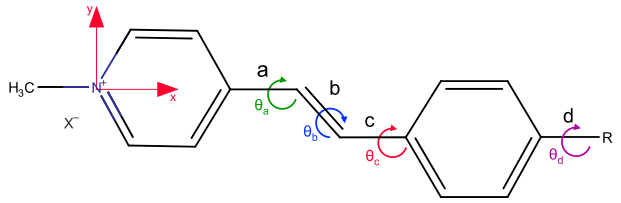

Complex:	**1** – R = H	X = I	**4.1** – R = N(n-Bu)$_2$	X = CF_3SO_3
	2 – R = tert-Bu	X = I	**4.2** – R = N(n-Bu)$_2$	X = ClO_4
	3 – R = N(Me)$_2$	X = I	**4.3** – R = N(n-Bu)$_2$	X = SCN
	4 – R = N(n-Bu)$_2$	X = I	**4.4** – R = N(n-Bu)$_2$	X = pTS [a]

Figure 1. Structure of the stilbazolium cations in the right-handed Cartesian frame and list of its anions. a, b, and c are the bonds used to determine the bond length alternation (BLA), and the θ's are the torsional angles around these respective bonds. The θ_d torsional angle is defined for complexes **3**, **4**, and **4.1**−**4.4** around the C−N bond. [a]p-toluenesulfonate.

description of the NLO responses of individual molecules in the gas phase or in solution, which can be performed reliably by considering the geometries of the stationary points on the potential energy surface,[12−15] a two-step multiscale approach known as Sequential-Quantum Mechanics/Molecular Mechanics[16,17] (S-QM/MM) is crucial to account for the distribution of the anions around the cation as well as to include the thermal and environmental effects on the NLO responses. In the first step, classical molecular dynamics (MD) simulations are performed to produce representative configurations of the complexes, and in a second step, quantum chemistry (QC) methods are used to evaluate the NLO responses of the selected configurations. Additionally, statistical analyses can quantify the relationships between the geometrical and the electronic properties leading to a better understanding of the phenomena. Following and adapting recent simulations of the NLO responses of solvated chromophores[18,19] as well as ion pairs,[10] sets of representative geometrical configurations of the solvated complexes in chloroform are sampled from classical MD simulations. The EFISHG responses are then calculated using the time-dependent density functional theory (TD-DFT) method. Additionally, the linear optical absorption and the hyper-Rayleigh scattering (HRS) responses are also computed. In order to reproduce the ground state geometries of the organic chromophores, the classical all-atom optimized potentials for liquid simulations[20] (OPLS-AA) force field (FF) was reparameterized and it was fitted to reproduce the DFT geometries. As will be demonstrated, the relative anion−cation position plays an important role in the EFISHG response due to its ability to modify the permanent dipole moment. On the other hand, the β tensor components are mostly independent of the relative anion−cation position.

This paper is organized as follows. Section 2 describes the essence of the computational aspects in the S-QM/MM multiscale procedure. Then, section 3 presents and discusses the results on the geometries, the linear and nonlinear optical properties, the relationships between them, as well as comparisons with experiments of ref 11. Finally, the conclusions are drawn in section 4.

2. COMPUTATIONAL ASPECTS

2.A. MD Simulations. Classical MD simulations were performed in a periodic cubic box adopting the NPT ensemble under ambient conditions (T = 298.15 K and P = 1 atm). The initial box containing the complex plus 1500 chloroform molecules was filled out and previously thermalized using the stochastic Monte Carlo Metropolis (MC) algorithm, with rigid molecular geometries, using the DICE[21] program. The initial setup for the MC simulation considers the fixed ion-pair geometry—obtained in the QM minimum energy while the chloroform molecules are randomly distributed. During this thermalization step, the geometry of the ion-pair complex was kept frozen. This procedure aims at avoiding undesired effects from initial nonequilibrium thermodynamics conditions. For each complex, the configuration after 2.25×10^8 MC steps was selected as the initial box for MD simulations with the Gromacs[22,23] software. In these MD simulations, the system is fully relaxed: the chromophore and anion geometries are fully flexible, including their relative positions. The MD equations were solved using the leapfrog algorithm for a total simulation time of 30 ns for the complexes with iodide anion (**1**−**4**) and for 50 ns otherwise (**4.1**−**4.4**), using a time step of 1 fs. An additional MD thermalization time of 5 ns was considered. Then, in the production step, the MD was run for 25 ns (45 ns) to provide the sampled configurations for the complexes **1**−**4** (**4.1**−**4.4**). The velocity rescaling thermostat[24] and the Parrinello−Rahman barostat[25] were respectively coupled every 100 and 1000 integration steps. A cutoff of 14.0 Å was defined for short-range nonbonding interactions while the smooth Particle-Mesh Ewald[26] method was used for long-range electrostatic corrections. The chloroform OPLS-AA force field proposed by McDonald[27] was employed.

Besides these simulations where the geometry of the chromophore is flexible, after the MC thermalization step, for complex **1**, an additional 4.5×10^8 MC steps were performed using rigid chromophore geometries in order to isolate the effects of the anion distribution around the cation from those of the dynamics of the chromophore geometry (the results from this simulation are identified as **1***).

The initial geometries of the complexes used in the MC simulations were obtained employing the energy minimization algorithm from Gaussian16[28] software at the IEFPCM/ωB97X-D/aug-cc-pVDZ level of calculation (IEFPCM - integral equation formalism of the polarizable continuum model[29,30]). The aug-cc-pVDZ pseudopotential basis set (named as aug-cc-pVDZ-PP) was used for iodine in all QC calculations. The ωB97X-D[31,32] exchange-correlation (XC) functional includes both long-range Hartree−Fock exchange and empirical London dispersion corrections, and its choice was validated comparing the results obtained with the second-order perturbative wave function MP2 method in the case of complexes **1** to **3**. The OPLS-AA FF parameters were used to describe the intra- and intermolecular interactions for the complexes in chloroform solution. Still, the equilibrium bond lengths and valence angles were modified to reproduce as closely as possible the QC equilibrium geometries of the complexes in chloroform, while the torsional parameters were

https://dx.doi.org/10.1021/acs.jcim.9b01161
J. Chem. Inf. Model. 2020, 60, 4817−4826

reparameterized to fit the QC energy profiles. The in-solution charges of the atomic sites of the chromophore−anion pairs, used in the classical simulations, were defined using IEFPCM/M06-2X/aug-cc-pVDZ/CHELPG electrostatic mapping.[33]

2.B. Nonlinear Optical Properties. The variations in the electric dipole moment upon the application of external electric fields define the linear and nonlinear optical properties named polarizability α, first β, and second γ hyperpolarizabilities. Adopting the T convention, their relationships can be expressed by

$$\begin{aligned}\Delta\mu_\zeta(-\omega_\sigma) = &\sum_{\eta}^{x,y,z} \alpha_{\zeta\eta}(-\omega_\sigma;\, \omega_1)E_\eta(\omega_1) \\ &+ \frac{1}{2!}\sum_{\eta,\chi}^{x,y,z} \beta_{\zeta\eta\chi}(-\omega_\sigma;\, \omega_1,\, \omega_2)E_\eta(\omega_1)E_\chi(\omega_2) \\ &+ \frac{1}{3!}\sum_{\eta,\chi,\xi}^{x,y,z} \gamma_{\zeta\eta\chi\xi}(-\omega_\sigma;\, \omega_1,\, \omega_2,\, \omega_3)E_\eta(\omega_1)E_\chi(\omega_2)E_\xi(\omega_3) + \ldots\end{aligned} \tag{1}$$

The electric field oscillating at an angular frequency ω_i applied in the η direction is represented by $E_\eta(\omega_i)$ and $\omega_\sigma = \sum_i \omega_i$. The α, β, and γ tensors are defined in the molecular axes coordinates ($\eta, \chi, \ldots = x, y, z$).[34] For compounds in solution, the EFISHG technique provides direct information on their first and second hyperpolarizabilities, according to[35]

$$\begin{aligned}\gamma_{\mathrm{EFISHG}} &= \langle\gamma(-2\omega;\, \omega,\, \omega,\, 0)\rangle \\ &= \gamma_{\parallel}(-2\omega;\, \omega,\, \omega,\, 0) + \frac{\mu\beta_{\parallel}(-2\omega;\, \omega,\, \omega)}{3kT} \\ &= \frac{[\mu\beta_{\parallel}(-2\omega;\, \omega,\, \omega)]_{\mathrm{eff}}}{3kT}\end{aligned} \tag{2}$$

where μ is the norm of the permanent ground state dipole moment and γ_{EFISHG} is the global EFISHG response. k is the Boltzmann constant, T is the temperature, and $3kT = 2.833 \times 10^{-3}$ a.u. at room temperature. The effective response, $[\mu\beta_{\parallel}]_{\mathrm{eff}}$, gathers both the second- and third-order contributions and is a useful quantity to compare with experimental results when the two contributions are not disentangled (this requires performing the measurements for a set of temperatures). From eq 2, the $\mu\beta_{\parallel}(-2\omega;\omega,\omega)/3kT$ term represents the second-order contribution to the global EFISHG response, also named the dipolar orientational contribution. The parallel β is often identified by $\beta_{\mathrm{EFISHG}}(-2\omega;\omega,\omega) = \beta_{\parallel}(-2\omega;\omega,\omega) = \beta_{\parallel}$, which corresponds to 3/5 times the projection of the vector component of the β tensor on the dipole moment axis:

$$\begin{aligned}\beta_{\parallel}(-2\omega;\, \omega,\, \omega) &= \frac{1}{5\mu}\sum_{\zeta}\mu_\zeta\sum_{\eta}(\beta_{\zeta\eta\eta} + \beta_{\eta\zeta\eta} + \beta_{\eta\eta\zeta}) \\ &= \frac{3}{5\mu}\sum_{\zeta}\mu_\zeta\beta_\zeta\end{aligned} \tag{3}$$

where μ_ζ is the ζth dipole moment Cartesian component and β_ζ is the ζth vector component of the first hyperpolarizability.

The $\gamma_{\parallel}(-2\omega;\omega,\omega,0)$ is the third-order contribution, which, in a first approximation, is often neglected in investigations on push−pull π-conjugated molecules. It is defined by the equation

$$\begin{aligned}\gamma_{\parallel}(-2\omega;\, \omega;\, \omega;\, 0) = \gamma_{\parallel} &= \frac{1}{15}\sum_{\zeta,\eta}(\gamma_{\zeta\zeta\eta\eta} + \gamma_{\zeta\eta\eta\zeta} + \gamma_{\zeta\eta\zeta\eta}) \\ &= \frac{1}{15}\sum_{\zeta,\eta}(2\gamma_{\zeta\zeta\eta\eta} + \gamma_{\zeta\eta\eta\zeta})\end{aligned} \tag{4}$$

The ratio $R_{3/2}$ between the second- and third-order contributions is used to estimate the weight of such contributions in the global EFISHG response. It is given by

$$R_{3/2} = 3kT \times \frac{\gamma_{\parallel}}{\mu\beta_{\parallel}} \tag{5}$$

An alternative technique to obtain information about the β response is the hyper-Rayleigh scattering (HRS) technique.[36] In typical HRS experimental setups, the vertically polarized scattered light is collected at a 90° angle with respect to the propagation direction and its intensity provides the $\beta^2_{\mathrm{HRS}}(-2\omega;\omega,\omega)$ quantity, which is the sum of two orientational averages, $\langle\beta^2_{ZZZ}\rangle$ and $\langle\beta^2_{ZXX}\rangle$:[37,38]

$$\beta_{\mathrm{HRS}}(-2\omega;\, \omega,\, \omega) = \sqrt{\langle\beta^2_{ZZZ}\rangle + \langle\beta^2_{ZXX}\rangle} \tag{6}$$

with

$$\begin{aligned}\langle\beta^2_{ZZZ}\rangle = \frac{1}{105}\sum_{\zeta\eta\chi}(&2\beta^2_{\zeta\eta\chi} + \beta_{\zeta\eta\eta}\beta_{\zeta\chi\chi} + 4\beta_{\zeta\zeta\eta}\beta_{\eta\chi\chi} + 4\beta_{\zeta\zeta\eta}\beta_{\chi\chi\eta} \\ &+ 4\beta_{\zeta\eta\chi}\beta_{\eta\zeta\chi})\end{aligned} \tag{7}$$

$$\begin{aligned}\langle\beta^2_{ZXX}\rangle = \frac{1}{105}\sum_{\zeta\eta\chi}(&6\beta^2_{\zeta\eta\chi} + 3\beta_{\zeta\eta\eta}\beta_{\zeta\chi\chi} - 2\beta_{\zeta\zeta\eta}\beta_{\eta\chi\chi} \\ &- 2\beta_{\zeta\zeta\eta}\beta_{\chi\chi\eta} - 2\beta_{\zeta\eta\chi}\beta_{\eta\zeta\chi})\end{aligned} \tag{8}$$

When considering vertically and horizontally polarized incident light, HRS measurements produce the depolarization ratio (DR), which provides information about the chromophore shape:[38]

$$\mathrm{DR} = \frac{\langle\beta^2_{ZZZ}\rangle}{\langle\beta^2_{ZXX}\rangle} \tag{9}$$

Note that lower-case indices refer to the molecular coordinates system while upper-case indices refer to the laboratory coordinates system.

2.C. NLO Calculations. The β and γ tensor components were calculated at the IEFPCM/M06-2X/6-311+G(d) QC level using the TD-DFT method on the 200 sampled configurations for each MD simulation. The aug-cc-pVDZ-PP basis set was used for the iodine atom. The M06-2X XC functional[39] has been selected owing to its performance for calculating the hyperpolarizabilities, in comparison to high-level wave function methods.[19,40,41] Owing to the large number of calculations, the 6-311+G(d) basis set for all atoms except iodine was selected based on its good accuracy with respect to larger basis sets.[41] This was further confirmed by additional calculations on complexes **1**−**4**, showing that β changes by less than 2−3% when using the 6-311+G(d,p) [polarization functions on the H atoms] or the more flexible aug-cc-pVDZ basis sets (Table S1). A dynamic electric field of 1907 nm wavelength was adopted, which is the same as in the experiments and which is far from electronic resonances. We then combined the NLO tensor components to obtain the set of NLO responses ($\beta_{\parallel}$, $\gamma_{\parallel}$, and β_{HRS}) for each configuration.

https://dx.doi.org/10.1021/acs.jcim.9b01161
J. Chem. Inf. Model. 2020, 60, 4817−4826

Finally, we evaluated the average and standard deviation of these NLO properties. From the sampled configurations, only the structures of the complexes were extracted, i.e., there are no explicit chloroform molecules in the QC NLO calculations. Nevertheless, the solute−solvent interactions were included using the IEFPCM. To highlight the β tensor component along the chromophore main or charge-transfer axis, after the MD simulations, the complexes were reorientated in the Cartesian axes as defined in Figure 1 before performing the TD-DFT calculations. All TD-DFT calculations were carried out using the Gaussian16 software.[28]

In addition, to analyze the second-order nonlinear optical responses, the vertical excitation energies and transition dipoles of the low-lying excited states were also calculated at the TD-DFT level, using the M06-2X XC functional and the 6-311+G(d) basis set. Like for the β and γ calculations, solvent effects were described using the IEFPCM scheme.

3. RESULTS AND DISCUSSION

3.A. Geometries. All ground state geometries used to parametrize the OPLS-AA force field were obtained employing the hybrid ωB97X-D XC functional and the aug-cc-pVDZ(-PP)—with pseudopotential for iodine—basis set. The minimum energy conditions were confirmed by the positive sign of the second-order derivatives of the energy with respect to vibrational normal coordinates. In these QC calculations, the chloroform solvent effects were approximated using the IEFPCM scheme. The validity of the ωB97X-D ground state geometries was assessed for the small complexes **1**−**3** by comparisons with the MP2 geometries. In addition to geometrical characteristics, atomic charges and NLO responses were also compared (Tables S2−S7 in the Supporting Information). An excellent agreement between both sets of geometries is observed, ensuring a reliable description of the minimum energy structure of the stilbazolium at the lower computational cost ωB97X-D level. The ionic character of the complexes was confirmed by the atomic charges calculated employing the CHELPG electrostatic mapping at the IEFPCM/M06-2X/aug-cc-pVDZ level. Indeed, the absolute values for the anions/cations charge (given by the sums of the atomic charges) amount to 0.91 for complexes **1**−**4** and to 0.92, 0.94, 0.95, and 0.95 for complexes **4.1**, **4.2**, **4.3**, and **4.4**, respectively. Additionally, moving the anion around the cation leads only to minor changes in the calculated atomic charges of the chromophore (mean absolute error ≤0.02 e), therefore substantiating the choice of the nonpolarizable OPLS-AA FF. Comparing the minimum energy geometries obtained with ωB97X-D and the reparameterized OPLS-AA force field, we observe (Table S2) a good agreement, indicating a robust reparameterization.

An accurate description of the bond length alternation (BLA = $[(a + c)/2 - b]$, defined here by the a, b, and c bonds, Figure 1) is needed for calculating reliable linear and nonlinear optical responses since the π-electron conjugation plays an important role in the description of the nonlocal electric field effects. This is especially the case for compounds presenting a push−pull character as well as for ion pairs, where the anion (and its position) can tune the intramolecular charge transfer. Besides the BLA, the cation−anion distance (d_{NA}) was considered. It is defined as the distance between the "positive" nitrogen atom of the cation and the A atom of the anion where A is I, S, Cl, C, and S for the I^-, $CF_3SO_3^-$, ClO_4^-, SCN^-, and pTS^- anions, respectively. This distance between the cation and the anion is an important structural property, later employed when searching for correlations with the electronic/optical properties. The BLA and d_{NA} values obtained from the sampled configurations and from the whole MD simulations are given in Table 1, together with the BLA of the minimum energy geometries that have been calculated at the DFT level. The distributions of the angles θ_a, θ_b, θ_c, and θ_d are presented in Figure S1.

Table 1. Average Values and Standard Deviations of the BLA (Å) and of the Nitrogen−Anion Distance (d_{NA}, Å) Obtained from the Sampled Configurations and from the Whole MD Simulations [Squared Brackets][a]

complex	BLA	d_{NA}
1*[b]	0.117 (0.117) [0.017]	4.340 ± 0.491 [4.336 ± 0.442]
1	0.114 ± 0.029 (0.117) [0.116 ± 0.030]	4.289 ± 0.412 [4.272 ± 0.390]
2	0.117 ± 0.031 (0.115) [0.115 ± 0.029]	4.280 ± 0.415 [4.277 ± 0.401]
3	0.099 ± 0.031 (0.098) [0.097 ± 0.030]	4.337 ± 0.366 [4.330 ± 0.376]
4	0.092 ± 0.028 (0.095) [0.094 ± 0.030]	4.450 ± 0.496 [4.357 ± 0.417]
4.1	0.095 ± 0.028 (0.094) [0.094 ± 0.030]	4.390 ± 0.440 [4.381 ± 0.450]
4.2	0.096 ± 0.030 (0.098) [0.098 ± 0.030]	4.400 ± 0.522 [4.396 ± 0.488]
4.3	0.097 ± 0.029 (0.098) [0.098 ± 0.030]	4.184 ± 0.535 [4.155 ± 0.546]
4.4	0.102 ± 0.031 (0.101) [0.101 ± 0.030]	4.273 ± 0.338 [4.280 ± 0.349]

[a]The BLA values of the minimum energy geometries obtained at the IEFPCM/ωB97X-D/aug-cc-pVDZ level are given in parentheses. [b]Rigid cation geometry calculations.

The BLA values are slightly smaller (by about 0.02 Å) for complexes **3** and **4** with respect to **1** and **2**. This shift is ascribed to the presence of the dialkylamino donor group. The difference between the average BLA values from the MD analyses and the BLA values from the ωB97X-D minimum energy geometries are not larger than 0.003 Å and within the standard deviations, substantiating the quality of the reparameterized FF. The effect of the anion nature is rather limited, though one notices an increase by up to 0.01 Å in the BLA values. The same trends were observed for the ωB97X-D minimum energy geometries as for the MD average values, both as a function of the cation and of its counteranion.

During the MD simulations, the ionic bond holds the anion moving around the cation with average values in agreement with the ωB97X-D minimum energy geometries. Any dissociations were not observed during the simulations. A superposition of the 200 sampled configurations for complexes **4** (the anion is I^-) and **4.4** (the anion is pTS^-) illustrates the distribution of the anion around the cation for the selected configurations (Figure 2). The reference d_{NA} value for complexes **1**−**4** obtained when the anion is in the same plane as the cation ring is 4.5 Å, while it goes down to 3.7 Å when it is above the N atom. The dependence of the average d_{NA} values as a function of either the cationic or anionic species is small in comparison to their standard deviations.

3.B. Excitation Energies. The IEFPCM/TD-DFT/M06-2X/6-311+G(d) method was employed to evaluate the vertical excitation energies (ΔE) and oscillator strengths (f) of the five

https://dx.doi.org/10.1021/acs.jcim.9b01161
J. Chem. Inf. Model. 2020, 60, 4817−4826

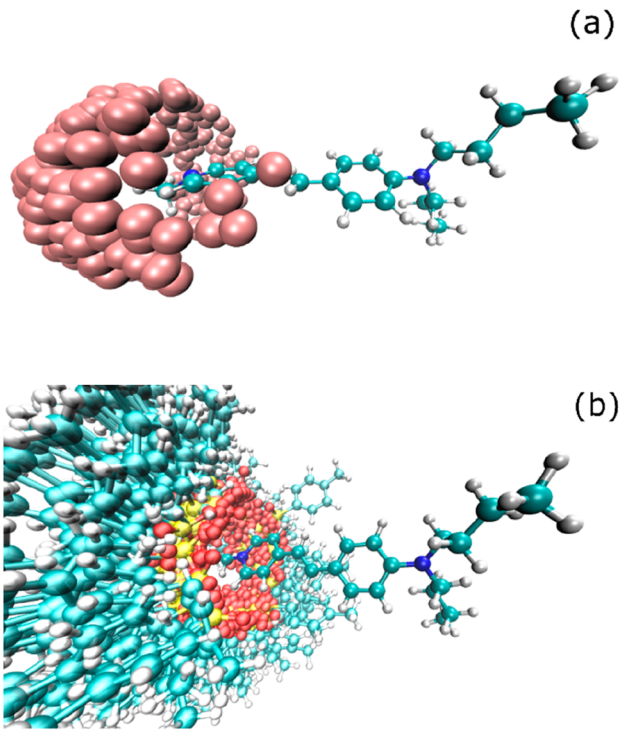

Figure 2. Relative position distribution of (a) the I^- and (b) the pTS^- anions around the positive site in complexes **4** and **4.4**. The geometries of the cations were taken at t = 5 ns, while a superposition of the 200 sampled configurations represents the anion distribution.

lowest-lying electronic transitions of all sampled configurations. To simulate the one-photon absorption (OPA) spectra, each transition was convoluted with a Lorentzian (L) broadening function with a half-width at half-maximum (HWHM) of 0.2 eV. So, for the nth configuration, the absorption intensity is defined as $I_n = \sum_{i=1}^{5} f_i \cdot L(\Delta E_i)$. Then, the total spectrum was obtained as the sum of the N = 200 configurations, as defined by $I = N^{-1}\sum_{n=1}^{200} I_n$. The maximum absorption intensity I_{max} defines the λ_{max} wavelength. In the case of complex **1**, I_{max} attains a value of 1.38, which was subsequently used to normalize the OPA spectra of all complexes.

Going from complex **1** to **4**, λ_{max} shifts from about 350 to 450 nm, while the relative maximum intensity increases by 21% (Table 2). The brightest excitations correspond to an intramolecular charge transfer transition from the donor phenyl or amino-phenyl ring to the acceptor pyridinium ring (Figure 3). Further details about these dominant excitations

Table 2. Experimental and Theoretical OPA Quantities[a]

complex	calculated λ_{max}	calculated I_{max}	experimental λ_{max}[b]
1*[c]	335	1.28	357
1	349	1.00	357
2	356	1.08	377
3	438	1.14	503
4	445	1.21	519
4.1	439	1.23	515
4.2	438	1.23	520
4.3	441	1.19	515
4.4	431	1.20	509

[a]Wavelengths (λ_{max}, expressed in nm) and maximum absorption intensities (I_{max}) were calculated at the IEFPCM/TD-DFT/M06-2X/6-311+G(d) level from the selected 200 snapshots. [b]From Tessore et al.[11] [c]Rigid cation geometry calculations.

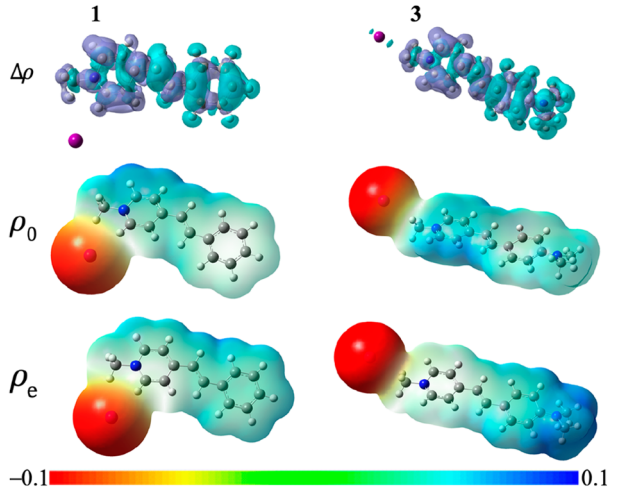

Figure 3. Excitation-induced electronic density difference ($\Delta\rho = \rho_e - \rho_0$) plots for complexes **1** and **3** together with their ground ρ_0 and excited ρ_e state densities. These were evaluated at the IEFPCM/TD-DFT/M06-2X/6-311+G(d) level. $\Delta\rho$ is represented by isosurfaces of value 0.0004 a.u. where blue color corresponds to a decrease of electron density upon excitation and violet corresponds to an increase. The electronic densities were colored by their respective electrostatic potential (a.u.).

are given by the pairs of occupied/unoccupied molecular orbitals that best describe these excitations (Figure S2). In all cases, this intense transition is driven by a $\pi-\pi^*$ excitation from the HOMO-x toward the LUMO. For complexes **1** and **2**, the electron is excited from the HOMO−3, and for complexes **3** to **4.4**, it is excited from HOMO, except for the complex **4.3** which is excited from HOMO−2. These frontier molecular orbitals are localized over the cation for all complexes. Note however that in the case of complexes **3** and **4**, the HOMO presents a weak contribution on the iodide, but this leads to negligible excitation-induced electronic density difference ($\Delta\rho = \rho_e - \rho_0$, where ρ_e and ρ_0 are the electron densities of the excited and ground states, respectively) contributions (Figure 3).

Increasing the OPA transition intensity while decreasing the transition energy should result in higher β values. This is predicted from the simplest two-state approximation,[42] where the dominant diagonal β tensor component (x is the direction of the charge transfer axis) is directly proportional to the square of the transition dipole moment and inversely proportional to the square of the excitation energy:

$$\beta_{xxx} = 6\frac{(\mu_e - \mu_0)_x \mu_{0e,x}^2}{\Delta E_{0e}^2} = 9\frac{(\mu_e - \mu_0)_x f_{0e}}{\Delta E_{0e}^3} \quad (10)$$

where $(\mu_e - \mu_0) = \Delta\mu_{0e}$ is the difference of dipole moment between the ground and dominant excited state, μ_{0e} is the transition dipole, ΔE_{0e} is the excitation energy, and f_{0e} is the oscillator strength of that transition (assumed to be dominated by the x component of μ_{0e}). This relationship is confirmed here since complexes **3** and **4** show larger β values than complexes **1** and **2** (*vide infra*). Again, the effects of the anion nature on the excitation energies and intensities are small,

https://dx.doi.org/10.1021/acs.jcim.9b01161
J. Chem. Inf. Model. 2020, 60, 4817−4826

Table 3. Calculated EFISHG and HRS First Hyperpolarizabilities at 1907 nm[a]

	$\mu\beta_{\parallel}$	$\beta_{\parallel}$	μ	$\theta_{(\mu,\beta)}$	β_{HRS}	DR
1*[b]	12 ± 17	1377 ± 1815	8.50 ± 0.89	71.6 ± 22.5	3552 ± 239	3.97 ± 0.41
1	13 ± 17	1404 ± 1895	8.47 ± 0.98	73.5 ± 21.3	3908 ± 616	3.83 ± 0.45
2	28 ± 25	3087 ± 2589	8.64 ± 0.92	65.5 ± 20.2	5592 ± 1024	4.13 ± 0.39
3	164 ± 72	16574 ± 6119	9.64 ± 1.01	49.9 ± 13.3	18341 ± 3699	4.66 ± 0.13
4	187 ± 109	18210 ± 9345	9.81 ± 1.20	51.6 ± 17.2	20942 ± 4856	4.69 ± 0.18
4.1	198 ± 81	20209 ± 6202	9.53 ± 1.35	46.6 ± 11.7	20746 ± 4091	4.87 ± 0.03
4.2	186 ± 96	18563 ± 7562	9.68 ± 1.41	50.1 ± 14.0	20810 ± 4173	4.87 ± 0.04
4.3	215 ± 93	21203 ± 6918	9.78 ± 1.51	44.2 ± 10.7	20760 ± 4691	4.78 ± 0.11
4.4	180 ± 75	21721 ± 6250	8.05 ± 1.48	38.1 ± 11.2	19483 ± 4188	4.85 ± 0.04

[a]Average responses and their standard deviations for $\mu\beta_{\parallel}$ (10^3 a.u.), $\beta_{\parallel}$ (a.u.), μ (a.u.), the $\theta_{(\mu,\beta)}$ angle between the μ and β vectors (deg.), β_{HRS} (a.u.), and its depolarization ratio (DR). [b]Rigid cation geometry calculations.

Table 4. Analyses of the Calculated EFISHG Responses at 1907 nm in Comparison to the Experimental $[\mu\beta_{\parallel}]$ (10^{-48} esu) Values[a]

	$\mu\beta_{\parallel}/3kT$	$\gamma_{\parallel}$	γ_{EFISHG}	$R_{3/2}$	$[\mu\beta_z]_{eff}$[b]	$[\mu\beta_z]_{eff}$(exp.)[b,c]
1*[d]	438 ± 584	60 ± 8	499 ± 583	0.064 ± 0.767	129 ± 151	800; 300; 170
1	460 ± 612	73 ± 15	533 ± 609	0.104 ± 1.364[e]	138 ± 158	800; 300; 170
2	993 ± 866	97 ± 16	1091 ± 868	0.051 ± 0.750	283 ± 225	810; 600; 205
3	5797 ± 2526	258 ± 43	6055 ± 2550	0.044 ± 0.134	1569 ± 661	1700; 1000; 1000
4	6596 ± 3831	303 ± 58	6899 ± 3863	0.026 ± 0.699	1788 ± 1001	1900; 1400; 1090
4.1	6973 ± 2857	272 ± 48	7245 ± 2993	0.045 ± 0.034	1878 ± 747	1150; 710; 225
4.2	6567 ± 3372	273 ± 48	6840 ± 3394	0.047 ± 0.046	1773 ± 880	1950; 1200; 250
4.3	7576 ± 3267	294 ± 58	7869 ± 3303	0.046 ± 0.020	2039 ± 856	1800; 1800; 1790
4.4	6351 ± 2658	265 ± 45	6616 ± 2685	0.048 ± 0.019	1715 ± 696	1150; 780; 690

[a]Average responses and their standard deviations for $\mu\beta_{\parallel}/3kT$, $\gamma_{\parallel}$, and γ_{EFISHG} (10^4 a.u.); $[\mu\beta_z]_{eff}$ (10^{-48} esu); and $R_{3/2} = (3kT \times \gamma_{\parallel})/\mu\beta_{\parallel}$. T = 298.15 K, $3kT = 2.833 \times 10^{-3}$ a.u. [b]Following ref 11, the $[\mu\beta_{\parallel}]_{eff}$ values are given within the X convention, with $[\mu\beta_z]_{eff,X} = 5/12[\mu\beta_{\parallel}]_{eff,T}$. [c]The experimental results are given for the successive 1×10^{-4}, 5×10^{-4}, and 1×10^{-3} M concentrations.[11] [d]Rigid cation geometry calculations [e]The snapshot with $R_{3/2} = -87$, corresponding to a negligible $\mu\beta_{\parallel}$ (because $\theta_{(\mu,\beta)} = 90.034°$), has not been taken into account for evaluating this average. When included, $R_{3/2} = -0.332 \pm 6.303$.

though one could notice a tendency: the excitation energy increases slightly with the size of the anion (Table 2).

The TD-DFT/M06-2X vertical excitation wavelengths reproduce the experimental trends of the variations of the maximum absorption wavelengths as a function of the phenyl substituent (R). On the other hand, they cannot account for the small variations resulting from varying the anion, which is consistent with the performance of the method.[43] Moreover, the calculated values are typically 0.1 to 0.4 eV larger than the experimental ones, in agreement with the expected 0.3 eV overestimation, as highlighted in a recent a TD-DFT benchmark review.[43] In all cases, the transition energies/wavelengths are far from possible resonances with the external electric field radiation (1907 and 954 nm for its second harmonic), avoiding spurious effects on the NLO responses.

3.C. EFISHG and HRS Responses. The calculated EFISHG and HRS responses are presented in Tables 3 and 4 together with their different contributions. The average $\mu\beta_{\parallel}$ values obtained for complexes **3** and **4** are about 1 order of magnitude larger than those of complexes **1** and **2**. Similarly, $\beta_{\parallel}$ increases from complexes **1** to **4**, whereas there are only small differences among the μ values, with the largest increase (~20%) between complexes **1** and **4**. These enhancements (of $\beta_{\parallel}$ and $\mu\beta_{\parallel}$) are first attributed to the presence of the amino donor groups on the terminal phenyl ring in agreement with their OPA spectra. The $\theta_{(\mu,\beta)}$ angle, between the μ and β vectors, also plays a role. It is smaller for the stronger donating substituents.

Considering complexes **4**–**4.4**, the $\beta_{\parallel}$ values increase following the I^-, ClO_4^-, $CF_3SO_3^-$, SCN^-, and pTS^- anion order, even though, considering their standard deviations, all values are statistically equivalent. The smallest average dipole moment is obtained for complex **4.4**, and therefore, although it exhibits the largest $\beta_{\parallel}$ value, its $\mu\beta_{\parallel}$ response is the lowest among the complexes **4**–**4.4**. The standard deviations of $\mu\beta_{\parallel}$ represent 131, 89, and 44% of their average values for complexes **1**–**3**, and 58, 41, 52, 43, and 42% for complexes **4**–**4.4**, respectively. Note that for the ion pairs formed between an acido-triggered indolino-oxazolidine and its trifluoroacetate counterion, even larger standard deviations relative to the average $\mu\beta_{\parallel}$ values were observed and were attributed to the quasi perpendicularity between the μ and β vectors.[10]

The average β_{HRS} values show the same trends as observed for $\beta_{\parallel}$ and $\mu\beta_{\parallel}$, but their standard deviations (relative to the average values) are smaller (16–23%). For perfect one-dimensional (1-D) NLOphores (having one dominant diagonal β tensor component aligned along the dipole moment axis), the $\beta_{\parallel} = 1.45\beta_{HRS}$ relationship is expected but this is clearly not the case in this study: the complexes **3** and **4** show similar $\beta_{\parallel}$ and β_{HRS} amplitudes, while for complexes **1** and **2** the $\beta_{\parallel}/\beta_{HRS}$ ratio amounts to 0.35–0.55 instead of 1.45. This originates from the facts that (i) the NLOphores are not purely 1-D (1-D NLOphores have DR = 5, while the DR values of cations **1** and **2** deviate most from this) and (ii) the μ and β vectors are not parallel with larger $\theta_{(\mu,\beta)}$ angles for complexes **1** and **2** in comparison to **3** and **4**. Note that the largest contribution to the $\mu\beta_{\parallel}$ values comes from the $\mu_x\beta_x$ component (the Cartesian axes are defined in Figure 1), and this relationship will be discussed later.

https://dx.doi.org/10.1021/acs.jcim.9b01161
J. Chem. Inf. Model. 2020, 60, 4817–4826

To disentangle the effects of the internal flexibility of the cation from those of the anion mobility on the EFISHG quantities, we performed, for complex **1**, extra simulations considering a rigid cation geometry, identified as **1***. The $\mu\beta_{\parallel}$ violin distributions of **1** and **1*** are similar (Figure 4). Similar

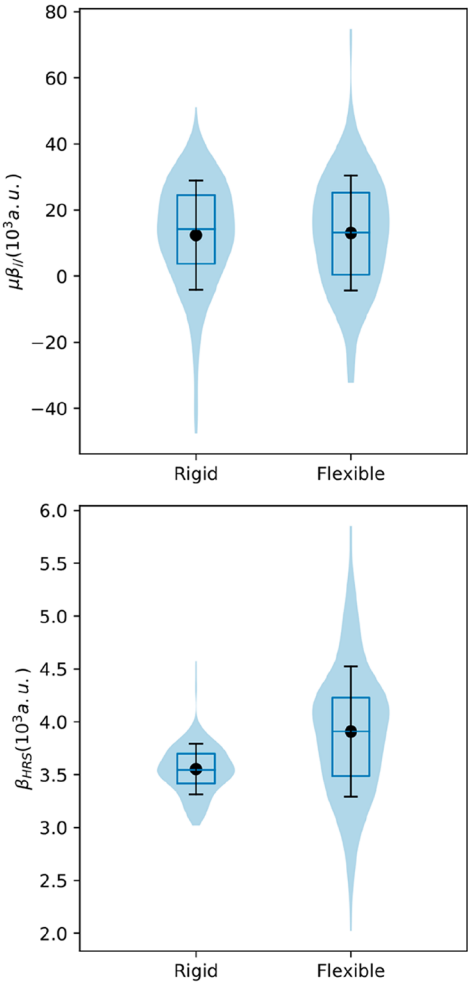

Figure 4. Violin distribution plots for (top) $\mu\beta_{\parallel}$ and (bottom) β_{HRS}, including the average (black point), the standard deviation (black lines), and the boxplot (blue lines indicating the first quartile at 25%, the median, and the third quartile at 75%) for complex **1** with or without rigid cation geometry. The calculations were performed at the IEFPCM/TD-DFT/M06-2X/6-311+G(d) level.

distributions are also observed for the corresponding μ as well as $\theta_{(\mu,\beta)}$ quantities (Table 3). In the case of β_{HRS}, their averages differ only by 10%, but their standard deviation is twice as large when the geometry is flexible in the MD simulations (Figure 4). Although neither the "rigid" nor the "flexible" distributions have Gaussian shapes, the average and the median values are almost equivalent (Figure 4), consistently with the EFISHG results. The whole set of violin distribution plots is presented in Figure S3.

Like the β quantities, (i) the $\gamma_{\parallel}$ values also increase when the stilbazolium is substituted by an amino donor group, which allows a push−pull effect; (ii) this increase amounts to a factor of 3−4; and (iii) the different anion species induce small changes in the $\gamma_{\parallel}$ values, again in comparison to the standard deviations (Table 4). When including the third-order $\gamma_{\parallel}$ contribution, the global EFISHG response increases by 15% and 10% for complexes **1** and **2**, respectively (Table 4, Figure 5). Although the $\gamma_{\parallel}$ value is larger in the presence of an amino

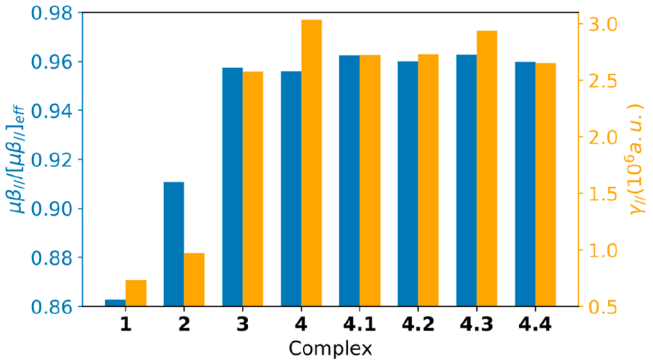

Figure 5. Ratio between the EFISHG responses including or not including the effects of the third-order $\gamma_{\parallel}$ contribution, $\mu\beta_{\parallel}/[\mu\beta_z]_{\mathrm{eff}}$, (blue) and the corresponding $\gamma_{\parallel}$ values (orange) as a function of the nature of the complex. All values have been calculated using the S-QM/MM scheme, and they correspond to the average quantities listed in Table 4.

group, the $\mu\beta_{\parallel}$ response is even larger so that the $R_{3/2}$ ratio reaches at most 5% for compounds **3** and **4**−**4.4**. In summary, the third-order NLO contribution to the EFISHG responses of the stilbazolium−anion complexes is small in comparison to its second-order counterpart, but yet, it is not negligible.

In the next step, we sought for correlations between the molecular properties (β_x, $\beta_{\parallel}$, β_{HRS}, μ_x, ΔE_{0e}, f_{0e}) and the geometrical parameters (BLA and X_{NA}, the x coordinate of d_{NA}). Pearson linear correlation (R coefficient) analyses demonstrate a weak correlation between β_x or β_{HRS} and the BLA amplitude, though it is globally slightly better in the latter case (Figure 6). The negative values of these $R(\beta - \mathrm{BLA})$ coefficients indicate that larger BLA values lead to smaller β responses. The R coefficients for the relationships between β_x or β_{HRS} and the torsion angles of the stilbazolium (θ_a, θ_b, θ_c, and θ_d) are smaller than 0.1, indicating no correlation, except maybe for the complex **4.1** (Figure S4). The weak or the absence of correlation between the β values and geometrical descriptors of the cation suggest a complex relationship between them that cannot be described by simple linear regression analyses.

On the other hand, there is a good correlation between β_x and $\beta_{\parallel}$, highlighting that the latter is mostly determined by the former. Then, interestingly, β_x is not influenced by the position of the anion along the x axis (X_{NA}), but $\beta_{\parallel}$ is strongly correlated with X_{NA} because μ_x appears to be almost fully determined by X_{NA}, i.e., by the anion position. Indeed, except for the large p-toluenesulfonate anion where the $R(\mu_x - X_{\mathrm{NA}}) = -0.77$, in all other cases, $|R|$ is larger than 0.95.

Then, correlations between the β_x values and the OPA properties ($1/\Delta E_{0e}^2$ and f_{0e}) confirm that the second-order NLO responses are, to a large extent, determined by the lowest-energy dipole-allowed transition. In these cases, the Pearson coefficients range from 0.6 to 0.9. Finally, the correlation between $1/\Delta E_{0e}^2$ and f_{0e} and the BLA was investigated, and it appears that the correlation is better for the $1/\Delta E_{0e}^2$ than for f_{0e}, with more negative R values in the former case.

3.D. Comparison with Experiment. The experimental EFISHG results of ref 11 show a large dependence of $[\mu\beta_{\parallel}]_{\mathrm{eff}}$

https://dx.doi.org/10.1021/acs.jcim.9b01161
J. Chem. Inf. Model. 2020, 60, 4817−4826

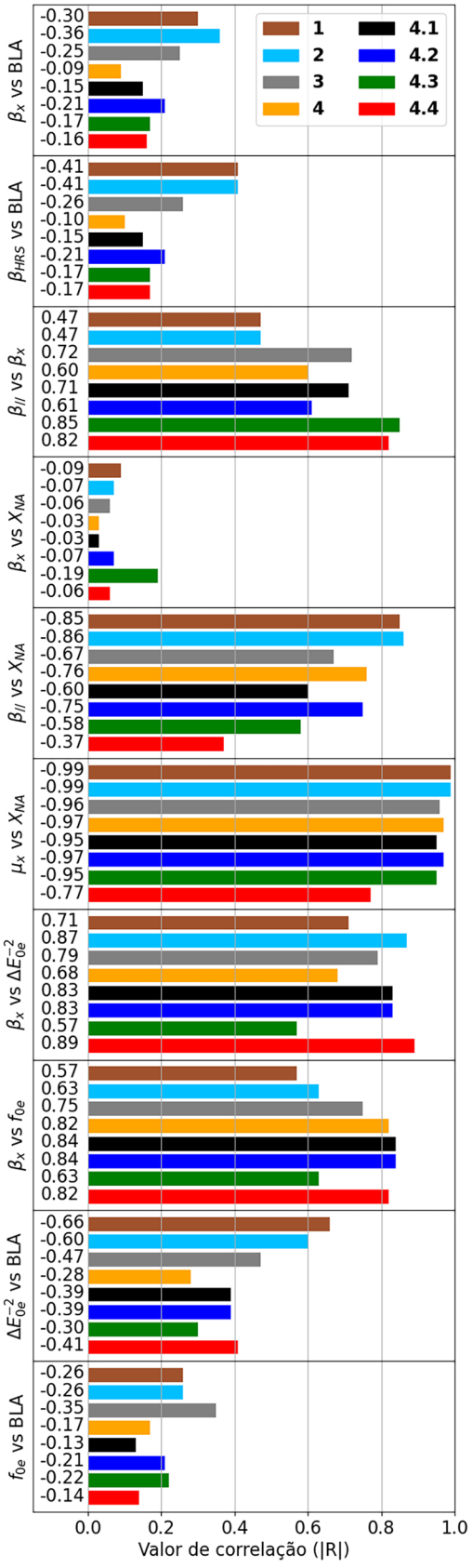

Figure 6. Linear correlation analyses between molecular properties (β_x, $\beta_{||}$, β_{HRS}, ΔE_{0e}, f_{0e}, and μ_x) and geometrical parameters (BLA and X_{NA}).

as a function of the concentration, adding difficulties to performing comparisons with the calculated values. These are however not related to the experimental error that was estimated to be about 10%.[11] The wide range of experimental values is related to the antagonistic effects of (i) the ion pairs dissociations and (ii) the chromophore aggregations. Indeed, at high concentrations, the chromophores (and their anions) can aggregate into centrosymmetric (or less noncentrosymmetric) structures, which present reduced first hyperpolarizabilities. On the other hand, at low concentrations, the ion pairs can (partly) dissociate, making difficult the measurements and leading to overestimated values. Of course, these effects are governed by the energies of association, which are determined by the ionic characters, the strengths of the van der Waals interactions, and the dielectric constant of the solution.

Considering this, the calculations reproduce well the variations of $[\mu\beta_{||}]_{eff}$ among the iodide complexes when considering the high concentration experimental data, i.e., smaller values with hydrogen or alkyl substituents (**1** and **2**) and larger ones with an amino group (**3** and **4**), especially. On the other hand, the small differences between the $[\mu\beta_{||}]_{eff}$ values of complexes **4**−**4.4**, as obtained from the calculations, are in better agreement with the low concentration experimental data. Moreover, in most cases, the experimental values are smaller than the calculated ones, figuring out a certain degree of aggregation.

4. CONCLUSIONS AND PERSPECTIVES

A Sequential-Quantum Mechanics/Molecular Mechanics (S-QM/MM) approach has been used to investigate the electric field-induced second harmonic generation (EFISHG) responses of ion pair complexes formed by stilbazolium cations and small- to medium-size counteranions. EFISHG is one of the techniques to describe the nonlinear optical responses of molecules in the gas phase and in solutions, and it works only for neutral species.[7,34,35] Therefore, for ions, the formation of neutral complexes is a prerequisite to carry out EFISHG measurements, and this is achieved by using weakly polar solvents like chloroform. Only a few studies have characterized the EFISHG responses of ion pairs,[8−11] including the work due to Tessore et al.[11] who have studied different ion pairs formed by stilbazolium cations and a series of small- to medium-size counteranions. However, the experimental EFISHG responses (γ_{EFISHG}) obtained in ref 11 depend strongly on the concentrations. This makes difficult the deduction of structure−property relationships and calls for complementary theoretical chemistry simulations to rationalize these results. Besides a recent work on the ion-pair formed by the acido-triggered indolino-oxazolidine and its trifluoroacetate counterion,[10] this work is the first computational chemistry investigation on the NLO responses of ion pairs and the first on the relationship between the NLO responses and the nature of the ions pairs. Contrary to the description of the NLO responses of individual molecules in the gas phase or in solution, which can be performed reliably by considering the geometries of the stationary points on the potential energy surface, a multiscale simulation approach was essential to including the spatial distribution of the anion around the cation as well as the thermal and environmental effects on the NLO responses and therefore to provide some insight into their variations.

https://dx.doi.org/10.1021/acs.jcim.9b01161
J. Chem. Inf. Model. 2020, 60, 4817−4826

Such a S-QM/MM approach has been optimized in order to scrutinize the NLO responses of these ion pairs and the simulations show that (i) γ_{EFISHG} is mostly determined by the second-order NLO contribution ($\mu\beta_{\parallel}$); (ii) $\mu\beta_{\parallel}$ depends strongly on the nature of the stilbazolium substituent, i.e., whether it is an amino donor group or not, with an increase by about 1 order of magnitude in the presence of an amino group; (iii) a part of this difference is attributed to the angle between the dipole moment and first hyperpolarizability vectors ($\theta_{(\mu,\beta)}$), which is mostly determined by the position of the anion with respect to the longitudinal charge-transfer axis of the stilbazolium; and (iv), on the other hand, the nature of the anion has little impact on $\mu\beta_{\parallel}$, and in all cases they are smaller than the standard deviations. Complementary β_{HRS} calculations substantiate the largest responses of the amino derivatives with respect to the other ones, but the differences are weaker because β_{HRS} does not depend on the dipole moment of the complex, nor on the position of the counteranion. Additional analyses have highlighted the dominant contribution of the low-energy charge-transfer excited state to the β responses, whereas no simple relationships have been unraveled between β and geometrical factors (bond length alternation and torsion angles).

Though the S-QM/MM approach is reliable to simulate the NLO responses of ion pairs notwithstanding the difficult comparison with the experimental data, there remain challenges to study the effects of chromophore aggregations and ion pair dissociations. Moreover, divalent cations/anions with different complex stoichiometries (anion/cation = 1:1 but also 2:1 and 1:2) should provide further understanding of the relationships between these complexes and their NLO responses. These constitute directions of further investigations.

■ ASSOCIATED CONTENT

Supporting Information

The Supporting Information is available free of charge at https://pubs.acs.org/doi/10.1021/acs.jcim.9b01161.

> Basis set effects on the $[\mu\beta_{\parallel}]_{eff}$ comparison between MP2 and ωB97X-D minimum energy geometries including CHELPG charges and NLO properties as determined at the IEFPCM/M06-2X/6-311+G(d) level, distributions of the key torsion angles, main molecular orbitals involved in the dominant low-energy dipole-allowed transition, violin distributions for $\mu\beta_{\parallel}$ and β_{HRS}, and correlation analyses for torsional angles (PDF)

■ AUTHOR INFORMATION

Corresponding Author

Benoît Champagne − *Theoretical Chemistry Lab, Unit of Theoretical and Structural Physical Chemistry, Namur Institute of Structured Matter, University of Namur, B-5000 Namur, Belgium;* orcid.org/0000-0003-3678-8875; Email: benoit.champagne@unamur.be

Authors

Tárcius N. Ramos − *Universidade de Sao Paulo, Instituto de Fisica, 05508-090 São Paulo, São Paulo, Brazil; Theoretical Chemistry Lab, Unit of Theoretical and Structural Physical Chemistry, Namur Institute of Structured Matter, University of Namur, B-5000 Namur, Belgium*

Sylvio Canuto − *Universidade de Sao Paulo, Instituto de Fisica, 05508-090 São Paulo, São Paulo, Brazil;* orcid.org/0000-0002-9942-8714

Complete contact information is available at: https://pubs.acs.org/10.1021/acs.jcim.9b01161

Notes

The authors declare no competing financial interest.

■ ACKNOWLEDGMENTS

This work was supported by grants 2015/14189-3 and 2018/17453-1 from São Paulo Research Foundation (FAPESP). The calculations were performed on the computing facilities of the Consortium des Équipements de Calcul Intensif (CÉCI, http://www.ceci-hpc.be) and of the University of Namur, on Zenobe, the Tier-1 facility of the Walloon Region (Convention 1117545).

■ REFERENCES

(1) Wagnière, G. H. *Linear and Nonlinear Optical Properties of Molecules*; Verlag Helvetica Chimica Acta: Basel, 1993.

(2) Campagnola, P. J.; Loew, L. M. Second-Harmonic Imaging Microscopy for Visualizing Biomolecular Arrays in Cells, Tissues and Organisms. *Nat. Biotechnol.* **2003**, *21*, 1356−1360.

(3) Andréasson, J.; Pischel, U. Molecules with a Sense of Logic: A Progress Report. *Chem. Soc. Rev.* **2015**, *44*, 1053−1069.

(4) Morel, Y.; Irimia, A.; Najechalski, P.; Kervella, Y.; Stephan, O.; Baldeck, P. L.; Andraud, C. Two-Photon Absorption and Optical Power Limiting of Bifluorene Molecule. *J. Chem. Phys.* **2001**, *114*, 5391−5396.

(5) Larson, D. R.; Zipfel, W. R.; Williams, R. M.; Clark, S. W.; Bruchez, M. P.; Wise, F. W.; Webb, W. W. Water-Soluble Quantum Dots for Multiphoton Fluorescence Imaging in Vivo. *Science* **2003**, *300*, 1434−1436.

(6) Kawata, S.; Sun, H. B.; Tanaka, T.; Takada, K. Finer Features for Functional Microdevices. *Nature* **2001**, *412*, 697−698.

(7) Levine, B. F.; Bethea, C. G. Second and Third Order Hyperpolarizabilities of Organic Molecules. *J. Chem. Phys.* **1975**, *63*, 2666−2682.

(8) Alain, V.; Blanchard-Desce, M.; Ledoux-Rak, I.; Zyss, J. Amphiphilic Polyenic Push−Pull Chromophores for Nonlinear Optical Applications. *Chem. Commun.* **2000**, *6*, 353−354.

(9) Cariati, E.; Dragonetti, C.; Lucenti, E.; Nisic, F.; Righetto, S.; Roberto, D.; Tordin, E. An Acido-Triggered Reversible Luminescent and Nonlinear Optical Switch Based on a Substituted Styrylpyridine: EFISH Measurements as an Unusual Method to Reveal a Protonation−Deprotonation NLO Contrast. *Chem. Commun.* **2014**, *50*, 1608−1610.

(10) Pielak, K.; Tonnelé, C.; Sanguinet, L.; Cariati, E.; Righetto, S.; Muccioli, L.; Castet, F.; Champagne, B. Dynamical Behavior and Second Harmonic Generation Responses in Acido-Triggered Molecular Switches. *J. Phys. Chem. C* **2018**, *122*, 26160−26168.

(11) Tessore, F.; Cariati, E.; Cariati, F.; Roberto, D.; Ugo, R.; Mussini, P.; Zuccaccia, C.; Macchioni, A. The Role of Ion Pairs in the Second-Order NLO Response of 4-X-1-Methylpiridinium Salts. *ChemPhysChem* **2010**, *11*, 495−507.

(12) Ferrighi, L.; Frediani, L.; Cappelli, C.; Sałek, P.; Ågren, H.; Helgaker, T.; Ruud, K. Density-Functional-Theory Study of the Electric-Field-Induced Second Harmonic Generation (EFISHG) of Push−Pull Phenylpolyenes in Solution. *Chem. Phys. Lett.* **2006**, *425*, 267−272.

(13) Suponitsky, K. Y.; Tafur, S.; Masunov, A. E. Applicability of Hybrid Density Functional Theory Methods to Calculation of Molecular Hyperpolarizability. *J. Chem. Phys.* **2008**, *129*, 044109.

(14) Pielak, K.; Bondu, F.; Sanguinet, L.; Rodriguez, V.; Champagne, B.; Castet, F. Second-Order Nonlinear Optical Properties of Multiaddressable Indolinooxazolidine Derivatives: Joint Computa-

tional and Hyper-Rayleigh Scattering Investigations. *J. Phys. Chem. C* **2017**, *121*, 1851−1860.
(15) Beaujean, P.; Champagne, B. Coupled Cluster Investigation of the Vibrational and Electronic Second and Third Harmonic Scattering Hyperpolarizabilities of the Water Molecule. *J. Chem. Phys.* **2019**, *151*, 064303.
(16) Coutinho, K.; Canuto, S. Solvent Effects from a Sequential Monte Carlo - Quantum Mechanical Approach. *Adv. Quantum Chem.* **1997**, *28*, 89−105.
(17) Coutinho, K.; Canuto, S.; Zerner, M. C. Monte Carlo-Quantum Mechanics Study of the Solvatochromic Shifts of the Lowest Transition of Benzene. *J. Chem. Phys.* **2000**, *112*, 9874−9880.
(18) Hidalgo Cardenuto, M.; Champagne, B. QM/MM Investigation of the Concentration Effects on the Second-Order Nonlinear Optical Responses of Solutions. *J. Chem. Phys.* **2014**, *141*, 234104.
(19) Hidalgo Cardenuto, M.; Champagne, B. The First Hyperpolarizability of Nitrobenzene in Benzene Solutions: Investigation of the Effects of Electron Correlation within the Sequential QM/MM Approach. *Phys. Chem. Chem. Phys.* **2015**, *17*, 23634−23642.
(20) Jorgensen, W. L.; Maxwell, D. S.; Tirado-Rives, J. Development and Testing of the OPLS All-Atom Force Field on Conformational Energetics and Properties of Organic Liquids. *J. Am. Chem. Soc.* **1996**, *118*, 11225−11236.
(21) Cezar, H. M.; Canuto, S.; Coutinho, K. *DICE(v3.0beta) A Monte Carlo Program for Molecular Liquid Simulation*; University of Sao Paulo: Brazil, 2018.
(22) Berendsen, H. J. C.; van der Spoel, D.; van Drunen, R. GROMACS: A Message-Passing Parallel Molecular Dynamics Implementation. *Comput. Phys. Commun.* **1995**, *91*, 43−56.
(23) Van Der Spoel, D.; Lindahl, E.; Hess, B.; Groenhof, G.; Mark, A. E.; Berendsen, H. J. C. GROMACS: Fast, Flexible, and Free. *J. Comput. Chem.* **2005**, *26*, 1701−1718.
(24) Bussi, G.; Donadio, D.; Parrinello, M. Canonical Sampling through Velocity Rescaling. *J. Chem. Phys.* **2007**, *126*, 014101.
(25) Parrinello, M.; Rahman, A. Crystal Structure and Pair Potentials: A Molecular-Dynamics Study. *Phys. Rev. Lett.* **1980**, *45*, 1196−1199.
(26) Essmann, U.; Perera, L.; Berkowitz, M. L.; Darden, T.; Lee, H.; Pedersen, L. G. A Smooth Particle Mesh Ewald Method. *J. Chem. Phys.* **1995**, *103*, 8577−8593.
(27) McDonald, N. A.; Carlson, H. A.; Jorgensen, W. L. Free Energies of Solvation in Chloroform and Water from a Linear Response Approach. *J. Phys. Org. Chem.* **1997**, *10*, 563−576.
(28) Frisch, M. J.; Trucks, G. W.; Schlegel, H. B.; Scuseria, G. E.; Robb, M. A.; Cheeseman, J. R.; Scalmani, G.; Barone, V.; Petersson, G. A.; Nakatsuji, X.; Li; Caricato, M.; Marenich, A. V.; Bloino, J.; Janesko, B. G.; Gomperts, R.; Mennucci, B.; Hratchian, H. P.; Ortiz, J. V.; Izmaylov, A. F.; Sonnenberg, J. L.; Williams-Young, D.; Ding, F.; Lipparini, F.; Egidi, F.; Goings, J.; Peng, B.; Petrone, A.; Henderson, T.; Ranasinghe, D.; Zakrzewski, V. G.; Gao, J.; Rega, N.; Zheng, G.; Liang, W.; Hada, M.; Ehara, M.; Toyota, K.; Fukuda, R.; Hasegawa, J.; Ishida, M.; Nakajima, T.; Honda, Y.; Kitao, O.; Nakai, H.; Vreven, T.; Throssell, K.; Montgomery, J. A., Jr.; Peralta, J. E.; Ogliaro, F.; Bearpark, M. J.; Heyd, J. J.; Brothers, E. N.; Kudin, K. N.; Staroverov, V. N.; Keith, T. A.; Kobayashi, R.; Normand, J.; Raghavachari, K.; Rendell, A. P.; Burant, J. C.; Iyengar, S. S.; Tomasi, J.; Cossi, M.; Millam, J. M.; Klene, M.; Adamo, C.; Cammi, R.; Ochterski, J. W.; Martin, R. L.; Morokuma, K.; Farkas, O.; Foresman, J. B.; Fox, D. J. *Gaussian16*, revision A.03, 2016.
(29) Mennucci, B.; Cammi, R.; Tomasi, J. Medium Effects on the Properties of Chemical Systems: Electric and Magnetic Response of Donor-Acceptor Systems within the Polarizable Continuum Model. *Int. J. Quantum Chem.* **1999**, *75*, 767−781.
(30) Tomasi, J.; Mennucci, B.; Cammi, R. Quantum Mechanical Continuum Solvation Models. *Chem. Rev.* **2005**, *105*, 2999−3094.
(31) Chai, J. Da; Head-Gordon, M. Long-Range Corrected Hybrid Density Functionals with Damped Atom-Atom Dispersion Corrections. *Phys. Chem. Chem. Phys.* **2008**, *10*, 6615−6620.
(32) Chai, J. Da; Head-Gordon, M. Systematic Optimization of Long-Range Corrected Hybrid Density Functionals. *J. Chem. Phys.* **2008**, *128*, 084106.
(33) Breneman, C. M.; Wiberg, K. B. Determining Atom-Centered Monopoles from Molecular Electrostatic Potentials. The Need for High Sampling Density in Formamide Conformational Analysis. *J. Comput. Chem.* **1990**, *11*, 361−373.
(34) Verbiest, T.; Clays, K.; Rodriguez, V. *Second-Order Nonlinear Optical Characterization Techniques*; CRC Press: New York, 2009, DOI: 10.1201/9781420070736.
(35) Ledoux, I.; Zyss, J. Influence of the Molecular Environment in Solution Measurements of the Second-Order Optical Susceptibility for Urea and Derivatives. *Chem. Phys.* **1982**, *73*, 203−213.
(36) Hendrickx, E.; Clays, K.; Persoons, A. Hyper-Rayleigh Scattering in Isotropic Solution. *Acc. Chem. Res.* **1998**, *31*, 675−683.
(37) Bersohn, R.; Pao, Y.-H.; Frisch, H. L. Double-Quantum Light Scattering by Molecules. *J. Chem. Phys.* **1966**, *45*, 3184−3198.
(38) Castet, F.; Bogdan, E.; Plaquet, A.; Ducasse, L.; Champagne, B.; Rodriguez, V. Reference Molecules for Nonlinear Optics: A Joint Experimental and Theoretical Investigation. *J. Chem. Phys.* **2012**, *136*, 024506.
(39) Zhao, Y.; Truhlar, D. G. The M06 Suite of Density Functionals for Main Group Thermochemistry, Thermochemical Kinetics, Noncovalent Interactions, Excited States, and Transition Elements: Two New Functionals and Systematic Testing of Four M06-Class Functionals and 12 Other Function. *Theor. Chem. Acc.* **2008**, *120*, 215−241.
(40) Castet, F.; Rodriguez, V.; Pozzo, J.-L.; Ducasse, L.; Plaquet, A.; Champagne, B. Design and Characterization of Molecular Nonlinear Optical Switches. *Acc. Chem. Res.* **2013**, *46*, 2656−2665.
(41) Champagne, B.; Beaujean, P.; de Wergifosse, M.; Cardenuto, M. H.; Liégeois, V.; Castet, F. Quantum Chemical Methods for Predicting and Interpreting Second-Order Nonlinear Optical Properties: From Small to Extended π-Conjugated Molecules. In *Frontiers of Quantum Chemistry*; Wojcik, M. J., Nakatsuji, H., Kirtman, B., Ozaki, Y., Eds.; Springer: Singapore, 2018; pp 117−138, DOI: 10.1007/978-981-10-5651-2_6.
(42) Papadopoulos, M., Sadlej, A., Leszczynski, J. *Non-Linear Optical Properties of Matter*; Springer Netherlands: Dordrecht, 2006, DOI: 10.1007/1-4020-4850-5.
(43) Laurent, A. D.; Jacquemin, D. TD-DFT Benchmarks: A Review. *Int. J. Quantum Chem.* **2013**, *113*, 2019−2039.

https://dx.doi.org/10.1021/acs.jcim.9b01161
J. Chem. Inf. Model. 2020, 60, 4817−4826